

# A Constrained Sequential-Lamination Algorithm for the Simulation of Sub-Grid Microstructure in Martensitic Materials

S. Aubry, M. Fago and M. Ortiz  
Graduate Aeronautical Laboratories  
California Institute of Technology  
Pasadena, CA 91125, USA

February 27, 2002

Submitted to: *Computer Methods in Applied Mechanics and Engineering*

Revised: October 10, 2002

## Abstract

We present a practical algorithm for partially relaxing multiwell energy densities such as pertain to materials undergoing martensitic phase transitions. The algorithm is based on sequential lamination, but the evolution of the microstructure during a deformation process is required to satisfy a continuity constraint, in the sense that the new microstructure should be reachable from the preceding one by a combination of branching and pruning operations. All microstructures generated by the algorithm are in static and configurational equilibrium. Owing to the continuity constrained imposed upon the microstructural evolution, the predicted material behavior may be path-dependent and exhibit hysteresis. In cases in which there is a strict separation of micro and macrostructural lengthscales, the proposed relaxation algorithm may effectively be integrated into macroscopic finite-element calculations at the subgrid level. We demonstrate this aspect of the algorithm by means of a numerical example concerned with the indentation of an Cu-Al-Ni shape memory alloy by a spherical indenter.

## Key words

martensitic phase transitions, relaxation, rank-one convexity, microstructure, sequential lamination, shape-memory alloys, indentation.

## 1 Introduction

Materials often are capable of adopting a multiplicity of crystal structures, or phases, the relative stability of which depends on temperature, the state of stress, and other factors. Under conditions

such that several phases are energetically favorable, e. g., at the transition temperature in martensitic materials, materials are often found to develop microstructure in nature or in the laboratory. A central problem in mechanics concerns the prediction of these microstructures and their effect on the effective or macroscopic behavior of materials, including such scaling properties and size effects as may result from their formation and evolution. When martensitic materials are modelled within the confines of nonlinear elasticity, the coexistence of phases confers their strain-energy density function a multiwell structure [26, 22, 14, 35]. The corresponding boundary value problems are characterized by energy functions which lack weak sequential lower-semicontinuity, and the energy-minimizing deformation fields tend to develop fine microstructure [7, 8, 23, 37].

There remains a need at present for efficient numerical methods for solving macroscopic boundary-value problems while simultaneously accounting for microstructure development at the microscale. One numerical strategy consists of attempting a direct minimization of a suitably discretized energy function. For instance, Tadmor *et al* [48] have applied this approach to the simulation of nanoindentation in silicon. The energy density is derived from the Stillinger-Weber potential by recourse to the Cauchy-Born approximation, and accounts for five phases of silicon. The energy functional is discretized by an application of the finite-element method. Tadmor *et al* [49] pioneering calculations predict the formation of complex phase arrangements under the indenter, and such experimentally observed features as an insulator-to-conductor transition at a certain critical depth of indentation.

Despite these successes, direct energy minimization is not without shortcomings. Thus, analysis has shown (see, e. g., [37] for a review) that the microstructures which most effectively relax the energy may be exceedingly intricate and, consequently, unlikely to be adequately resolved by a fixed numerical grid. As a result, the computed microstructure is often coarse and biased by the computational mesh, which inhibits—or entirely suppresses—the development of many of the competing microstructures. By virtue of these constraints, the numerical solution is often caught up in a metastable local minimum which may not accurately reflect the actual energetics and deformation characteristics of the material.

In applications where there is a clear separation of micro and macrostructural lengthscales, an alternative numerical strategy is to use a suitably relaxed energy density in calculations [20, 36, 10, 24, 27]. In this approach, the original multiwell energy density is replaced by its *quasiconvex* envelop, i. e., by the lowest energy density achievable by the material through the development of microstructure. Thus, the determination of the relaxed energy density requires the evaluation of *all* possible microstructures compatible with a prescribed macroscopic deformation. The resulting relaxed energy density is quasiconvex [37], and its minimizers, which represent the macroscopic deformation fields, are devoid of microstructure and, thus, more readily accessible to numerical methods. In essence, the use of relaxed energy densities in macroscopic boundary value problems constitutes a multiscale approach in which the development of microstructure occurs—and is dealt with—at the *subgrid* level. The central problem in this approach is to devise effective means of determining the relaxed energy density and of integrating it into macroscopic calculations.

Unfortunately, no general algorithm for the determination of the quasiconvex envelop of an arbitrary energy density is known at present. A fallback strategy consists of the consideration of *special* microstructures only, inevitably resulting in a partial relaxation of the energy density. For instance, attention may be restricted to microstructures in the form of *sequential laminates* [31, 36, 39, 40, 25, 24]. The lowest energy density achievable by the material through sequential

lamination is known as the *rank-one* convexification of the energy density. Many of the microstructures observed in shape-memory alloys [22] and in ductile single crystals [39] may be interpreted as instances of sequential lamination, which suggests that the rank-one convexification of the energy coincides—or closely approximates—the relaxed energy for these materials. Ductile single crystals furnish a notable example in which the rank-one and the quasiconvex envelopes are known to coincide exactly [5].

In this paper we present a practical algorithm for partially relaxing multiwell energy densities. The algorithm is based on sequential lamination and, hence, at best it returns the rank-one convexification of the energy density. Sequential lamination constructions have been extensively used in both analysis and computation [31, 8, 14, 29, 36, 39, 34, 3, 4]. All microstructures generated by the algorithm are in static and configurational equilibrium. Thus, we optimize all the interface orientations and variant volume fractions, with the result that all configurational forces and torques are in equilibrium. We additionally allow the variants to be arbitrarily stressed and enforce traction equilibrium across all interfaces.

The proposed lamination construction is *constrained* in an important respect: during a deformation process, we require that every new microstructure be reachable from the preceding microstructure along an admissible transition path. The mechanisms by which microstructures are allowed to effect topological transitions are: *branching*, i. e., the splitting of a variant into a rank-one laminate; and *pruning*, consisting of the elimination of variants whose volume fraction reduces to zero. Branching transitions are accepted provided that they reduce the total energy, without consideration of energy barriers. By repeated branching and pruning microstructures are allowed to evolve along a deformation process. The *continuation* character of the algorithm furnishes a simple model of metastability and hysteresis. Thus, successive microstructures are required to be ‘close’ to each other, which restrict the range of microstructures accessible to the material at any given time. In general, this restriction causes the microstructures to be path-dependent and metastable, and the computed macroscopic response may exhibit hysteresis.

The proposed relaxation algorithm may effectively be integrated into macroscopic finite-element calculations at the subgrid level. We demonstrate the performance and versatility of the algorithm by means of a numerical example concerned with the indentation of an Cu-Al-Ni shape memory alloy [22] by a spherical indenter. The calculations illustrate the ability of the algorithm to generate complex microstructures while simultaneously delivering the macroscopic response of the material. In particular, the algorithm results in force-depth of indentation curves considerably softer than otherwise obtained by direct energy minimization.

## 2 Problem Formulation

Let  $\Omega \in \mathbb{R}^3$  be a bounded domain representing the reference configuration of the material. Let  $\mathbf{y}(x) : \Omega \rightarrow \mathbb{R}^3$  be the deformation and  $\mathbf{F}(x) = D\mathbf{y}(x)$  be the corresponding deformation gradient. We denote the elastic energy density at deformation gradient  $\mathbf{F} \in \mathbb{R}^{3 \times 3}$  by  $W(\mathbf{F})$ . We require  $W(\mathbf{F})$  to be material frame indifferent, i. e., to be such that  $W(\mathbf{R}\mathbf{F}) = W(\mathbf{F})$ ,  $\forall \mathbf{R} \in SO(3)$  and  $\mathbf{F} \in \mathbb{R}^{3 \times 3}$ . In addition, the case of primary interest here concerns materials such that  $W(\mathbf{F})$  is not quasiconvex. As a simple example, we may suppose that  $W(\mathbf{F})$  has the following special structure: Let  $W_i(\mathbf{F})$ ,  $i = 1, \dots, M$  be quasiconvex energy densities (see, e. g., [23] for a definition

and discussion of quasiconvexity), representing the energy wells of the material. Then

$$W(\mathbf{F}) = \min_{m=0,\dots,M} W_m(\mathbf{F}) \quad (1)$$

i. e.,  $W(\mathbf{F})$  is the lower envelop of the functions  $W_m(\mathbf{F})$ .

A common model of microstructure development in this class of materials presumes that the microstructures of interest correspond to low-energy configurations of the material, and that, consequently, their essential structure may be ascertained by investigating the absolute minimizers of the energy. However, the energy functionals resulting from multiwell energy densities such as (1) lack weak-sequential lower semicontinuity and their infimum is not attained in general [23]. The standard remedy is to introduce the quasiconvex envelop

$$QW(\mathbf{F}) = \frac{1}{|Q|} \inf_{\mathbf{u} \in W_0^{1,\infty}(Q)} \int_Q W(\mathbf{F} + D\mathbf{u}) dx \quad (2)$$

of  $W(\mathbf{F})$ , or relaxed energy density. In this expression,  $W_0^{1,\infty}(Q)$  denotes the space of functions whose distributional derivatives are essentially bounded and which vanish on the boundary, and  $Q$  is an arbitrary domain. Physically,  $QW(\mathbf{F})$  represents the lowest energy density achievable by the material through the development of microstructure. The macroscopic deformations of the solid are then identified with the solutions of the relaxed problem:

$$\inf_{\mathbf{y} \in X} \left\{ \int_{\Omega} [QW(D\mathbf{y}) - \mathbf{f} \cdot \mathbf{y}] dx - \int_{\partial\Omega_2} \bar{\mathbf{t}} \cdot \mathbf{y} \right\} \quad (3)$$

where  $X$  denotes some suitable solution space,  $\mathbf{f}$  is a body force field,  $\mathbf{t}$  represents a distribution of tractions over the traction boundary  $\partial\Omega_2$ , and the deformation of the body is constrained by displacement boundary conditions of the form:

$$\mathbf{y} = \bar{\mathbf{y}} \text{ on } \partial\Omega_1 = \partial\Omega - \partial\Omega_2 \quad (4)$$

Thus, in this approach the effect of microstructure is built into the relaxed energy  $QW(\mathbf{F})$ . The relaxed problem defined by  $QW(\mathbf{F})$  then determines the macroscopic deformation.

In executing this program the essential difficulty resides in the determination of the relaxed energy  $QW(\mathbf{F})$ . As mentioned in the introduction, no general algorithm for the determination of the quasiconvex envelop of an arbitrary energy density is known at present. A fallback strategy is to effect a partial relaxation of the energy density by recourse to *sequential lamination* [31, 36], and the use of the resulting rank-one convexification  $RW(\mathbf{F})$  of  $W(\mathbf{F})$  in lieu of  $QW(\mathbf{F})$  in the macroscopic variational problem (3). We recall that the rank-one convexification  $RW(\mathbf{F})$  of  $W(\mathbf{F})$  follows as the limit [32, 33]

$$RW(\mathbf{F}) = \lim_{k \rightarrow \infty} R_k W(\mathbf{F}) \quad (5)$$

where  $R_0 W(\mathbf{F}) = W(\mathbf{F})$  and  $R_k W(\mathbf{F})$  is defined recursively as

$$R_k W(\mathbf{F}) = \inf_{\lambda, \mathbf{a}, \mathbf{N}} \{ (1 - \lambda) R_{k-1} W(\mathbf{F} - \lambda \mathbf{a} \otimes \mathbf{N}) + \lambda R_{k-1} W(\mathbf{F} + (1 - \lambda) \mathbf{a} \otimes \mathbf{N}), \quad (6)$$

$$\lambda \in [0, 1], \mathbf{a}, \mathbf{N} \in \mathbb{R}^3, |\mathbf{N}| = 1 \} \quad k \geq 1$$

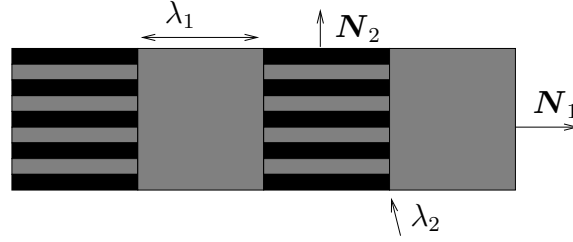


Figure 1: Example of a rank-2 laminate.  $\lambda_1$  and  $\lambda_2$  are the volume fractions corresponding to levels 1 and 2, respectively, and  $N_1$  and  $N_2$  are the corresponding unit normals.

In these expressions,  $\lambda$  and  $1 - \lambda$  represent the volume fractions of the  $k$ -level variants,  $N$  is the unit normal to the planar interface between the variants, and  $\mathbf{a}$  is a vector (see Fig. 1).

Unfortunately, a practical algorithm for the evaluation of the rank-one convexification of general energy densities ‘on the fly’ does not appear to be available at present. Dolzmann [25] has advanced a method for the computation of the exact rank-one convexification of an arbitrary energy density in two dimensions. However, extensions of the method to three dimensions do not appear to be available at present. In addition, the method requires the *a priori* tabulation of  $RW(\mathbf{F})$  over all of  $\mathbb{R}^{2 \times 2}$ , which limits its applicability to large-scale computing.

An additional complication arises from the fact that the cyclic behavior of martensitic materials often exhibits hysteresis. Under these conditions, the response of the material is path-dependent and dissipative, and, therefore, absolute energy minimization does not furnish a complete model of material behavior. The modeling of hysteresis requires consideration of entire deformation processes, rather than isolated states of deformation of the material. A framework for the understanding of hysteresis may be constructed by assuming that the evolution of microstructure is subject to a *continuity* requirement, namely, to the requirement that successive microstructures be close to each other in some appropriate sense. This constraint restricts the range of microstructures which the material may adopt at any given time and thus results in metastable configurations. The particular sequence of metastable configurations adopted by the material may be path dependent, resulting in hysteresis. The connection between metastability and hysteresis has been discussed by Ball, Chu and James [9].

### 3 A sequential lamination algorithm

The problem which we address in the remainder of this paper concerns the formulation of efficient algorithms for the evaluation of  $RW(\mathbf{F})$ , and extensions thereof accounting for kinetics and nonlocal effects, with specific focus on algorithms which can be effectively integrated into large-scale macroscopic simulations. We begin by reviewing basic properties of sequential laminates for subsequent reference. More general treatments of sequential lamination may be found in [33, 31, 12, 13, 44, 36].

Uniform deformations may conventionally be categorized as rank-zero laminates. A rank-one laminate is a layered mixture of two deformation gradients,  $\mathbf{F}^-, \mathbf{F}^+ \in \mathbb{R}^{3 \times 3}$ . Compatibility of

deformations then requires  $\mathbf{F}^\pm$  to be rank-one connected, i. e.,

$$\mathbf{F}^+ - \mathbf{F}^- = \mathbf{a} \otimes \mathbf{N} \quad (7)$$

where  $\mathbf{a} \in \mathbb{R}^3$ , and  $\mathbf{N} \in \mathbb{R}^3$ ,  $|\mathbf{N}| = 1$ , is the normal to the interface between the two variants of deformation. Let  $\lambda^\pm$ ,

$$\lambda^- + \lambda^+ = 1, \quad \lambda^\pm \in [0, 1], \quad (8)$$

denote the volume fractions of the variants. Then, the average or macroscopic deformation follows as

$$\mathbf{F} = \lambda^- \mathbf{F}^- + \lambda^+ \mathbf{F}^+ \quad (9)$$

If  $\mathbf{F}$  and  $\{\mathbf{a}, \lambda^\pm, \mathbf{N}\}$  are known, then the deformation in the variants is given by:

$$\begin{aligned} \mathbf{F}^+ &= \mathbf{F} + \lambda^- \mathbf{a} \otimes \mathbf{N} \\ \mathbf{F}^- &= \mathbf{F} - \lambda^+ \mathbf{a} \otimes \mathbf{N}. \end{aligned} \quad (10)$$

and, thus,  $\mathbf{F}$  and  $\{\mathbf{a}, \lambda^\pm, \mathbf{N}\}$  define a complete set of deformation and configurational-degrees of freedom for the laminate. Following Kohn [31], a laminate of rank- $k$  is a layered mixture of two rank- $(k-1)$  laminates, which affords an inductive definition of laminates of any rank. As noted by Kohn [31], the construction of sequential laminates assumes a separation of scales: the length scale  $l_k$  of the  $k$ th-rank layering satisfies  $l_k \ll l_{k-1}$ .

Sequential laminates have a binary-tree structure. Indeed, with every sequential laminate we may associate a *graph*  $G$  such that: the nodes of  $G$  consist of all the sub-laminates of rank less or equal to the rank  $k$  of the laminate; and joining each sub-laminate of order  $1 \leq l \leq k$  with its two constituent sub-laminates of order  $l-1$ . The root of the graph is the entire laminate. Two sequential laminates will be said to have the same *structure* (alternatively, *topology* or *layout*) if their graphs are identical. Evidently, having the same structure defines an equivalence relation between sequential laminates, and the set of all equivalence classes is in one-to-one correspondence with the set  $\mathcal{B}$  of binary trees.

Let  $i = 1, \dots, n$  be an enumeration of the nodes of  $G$ . Then, to each node  $i$  we may associate a deformation  $\mathbf{F}_i$ . The root deformation is the average or macroscopic deformation  $\mathbf{F}$ . Each node in the tree has either two children or none at all. Nodes with a common parent are called siblings. Nodes without children are called leaves. Nodes which are not leaves are said to be interior. The deformations of the children of node  $i$  will be denoted  $\mathbf{F}_i^\pm$ . Each generation of nodes is called a level. The root occupies level 0 of the tree. The number of levels is the rank  $k$  of the tree. Level  $l$  contains at most  $2^l$  nodes. The example in Fig. 2 represents a rank-two laminate of order four. The three leaves of the tree are nodes  $\mathbf{F}^+$ ,  $\mathbf{F}^{-+}$  and  $\mathbf{F}^{--}$ . The interior nodes are  $\mathbf{F}$  and  $\mathbf{F}^-$ . The children of, e. g., node  $\mathbf{F}^-$  are nodes  $\mathbf{F}^{-+}$  and  $\mathbf{F}^{--}$ .

Compatibility demands that each pair of siblings be rank-one connected, i. e.,

$$\mathbf{F}_i^+ - \mathbf{F}_i^- = \mathbf{a}_i \otimes \mathbf{N}_i, \quad i \in \mathcal{I}_G \quad (11)$$

where  $\mathbf{a}_i \in \mathbb{R}^3$ ,  $\mathbf{N}_i \in \mathbb{R}^3$ ,  $|\mathbf{N}_i| = 1$ , is the normal to the interface between  $\mathbf{F}_i^-$  and  $\mathbf{F}_i^+$ , and  $\mathcal{I}_G$  denotes the set of all interior nodes. Let  $\lambda_i^\pm$ ,

$$\lambda_i^- + \lambda_i^+ = 1, \quad \lambda_i^\pm \in [0, 1], \quad (12)$$

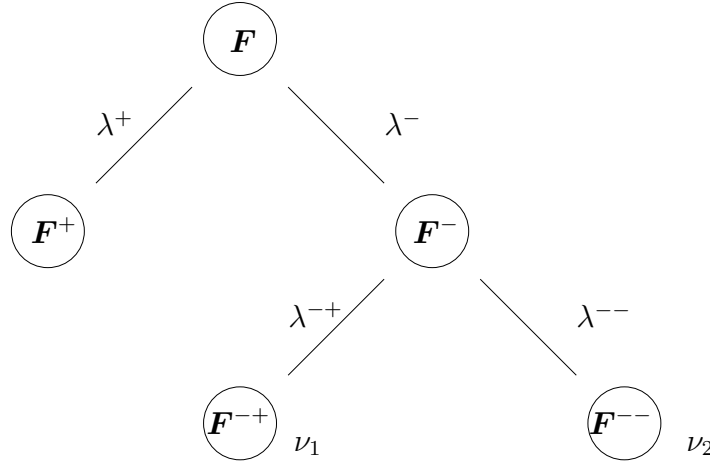


Figure 2: *Example of a rank-2 laminate. In this example,  $\nu_1 = \lambda^- \lambda^{-+}$  and  $\nu_2 = \lambda^- \lambda^{--}$ .*

denote the volume fractions the variants  $\mathbf{F}_i^\pm$  within node  $i$ . Then, the deformation of the parent variant is recovered in the form

$$\mathbf{F}_i = \lambda_i^- \mathbf{F}_i^- + \lambda_i^+ \mathbf{F}_i^+ \quad (13)$$

If  $\mathbf{F}_i$  and  $\{\mathbf{a}_i, \lambda_i^\pm, \mathbf{N}_i\}$  are known for an interior node  $i$ , then the deformation of its children is given by:

$$\begin{aligned} \mathbf{F}_i^+ &= \mathbf{F}_i + \lambda_i^- \mathbf{a}_i \otimes \mathbf{N}_i \\ \mathbf{F}_i^- &= \mathbf{F}_i - \lambda_i^+ \mathbf{a}_i \otimes \mathbf{N}_i. \end{aligned} \quad (14)$$

Therefore,  $\mathbf{F}$  and  $\{\mathbf{a}_i, \lambda_i^\pm, \mathbf{N}_i, i \in \mathcal{I}\}$  define a complete and independent set of degrees of freedom for the laminate. A recursive algorithm for computing all the variant deformations  $\mathbf{F}_i, i = 1, \dots, n$  from  $\mathbf{F}$  and  $\{\mathbf{a}_i, \lambda_i^\pm, \mathbf{N}_i, i \in \mathcal{I}_G\}$  has been given by [40].

We shall also need the global volume fractions  $\nu_l$  of all leaves  $l \in \mathcal{L}_G$ , where  $\mathcal{L}_G$  denotes the collection of all leaves of  $G$ . These volume fractions are obtained recursively from the relations:

$$\nu_i^\pm = \lambda_i^\pm \nu_i, \quad i \in \mathcal{I}_G \quad (15)$$

with  $\nu_{\text{root}} = 1$  for the entire laminate, and satisfy the relation:

$$\sum_{l \in \mathcal{L}_G} \nu_l = 1 \quad (16)$$

Thus,  $\nu_l$  represents the volume occupied by leaf  $l$  as a fraction of the entire laminate. The Young measure (e. g., [37]) of the laminate consist of a convex combination of atoms  $\delta_{\mathbf{F}_l}(\mathbf{F})$  with weights  $\nu_l, l \in \mathcal{L}$ .

The average or macroscopic stress of the laminate may be expressed in the form

$$\mathbf{P} = \sum_{l \in \mathcal{L}_G} \nu_l \mathbf{P}_l \quad (17)$$

where

$$\mathbf{P}_l = W_{,\mathbf{F}}(\mathbf{F}_l), \quad l \in \mathcal{L}_G \quad (18)$$

are the first Piola-Kirchhoff stresses in the leaves. The average stress may be computed by recursively applying the averaging relation:

$$\mathbf{P}_i = \lambda^- \mathbf{P}_i^- + \lambda^+ \mathbf{P}_i^+, \quad i \in \mathcal{I} \quad (19)$$

starting from the leaves of the laminate. A recursive algorithm for computing the average stress  $\mathbf{P}$  from  $\{\mathbf{P}_l, l \in \mathcal{L}\}$  and  $\{\lambda_i^\pm, i \in \mathcal{I}_G\}$  has been given by [40].

### 3.1 Microstructural equilibrium

We begin by investigating the mechanical and configurational equilibrium of sequential laminates of given structure. Thus, we consider an elastic material of strain-energy density  $W(\mathbf{F})$  subject to a prescribed macroscopic deformation  $\mathbf{F} \in \mathbb{R}^{3 \times 3}$ . In addition, we consider all sequential laminates with given graph  $G$ .

The equilibrium configurations of the laminate then follow as the solutions of the constrained minimization problem:

$$GW(\mathbf{F}) = \inf_{\{\mathbf{a}_i, \lambda_i^\pm, \mathbf{N}_i, i \in \mathcal{I}_G\}} \sum_{l \in \mathcal{L}_G} \nu_l W(\mathbf{F}_l) \quad (20)$$

$$\lambda_i^\pm \in [0, 1], \quad i \in \mathcal{I}_G \quad (21)$$

$$|\mathbf{N}_i| = 1, \quad i \in \mathcal{I}_G \quad (22)$$

where the  $\mathbf{F}_l$  are obtained from the recursive relations (14). The effective or macroscopic energy of the laminate is  $GW(\mathbf{F})$ . If  $W(\mathbf{F})$  is quasiconvex then it necessarily follows that  $\mathbf{a}_i = \mathbf{0}, \forall i \in \mathcal{I}_G$ , and  $GW(\mathbf{F}) = W(\mathbf{F})$ .

It is interesting to verify that the solutions of the minimization problem (20) are in both force and configurational equilibrium. Thus, assuming sufficient smoothness, the stationarity of the energy with respect to all deformation jump amplitudes yields the traction equilibrium equations:

$$(\mathbf{P}_i^+ - \mathbf{P}_i^-) \cdot \mathbf{N}_i = \mathbf{0}, \quad i \in \mathcal{I}_G \quad (23)$$

Stationarity with respect to all normal vectors yields the configurational-torque equilibrium equations:

$$[\mathbf{a}_i \cdot (\mathbf{P}_i^+ - \mathbf{P}_i^-)] \times \mathbf{N}_i = \mathbf{0}, \quad i \in \mathcal{I}_G \quad (24)$$

Finally, stationarity with respect to all volume fractions yields the configurational-force equilibrium equations:

$$f_i = (W_i^+ - W_i^-) - (\lambda_i^+ \mathbf{P}_i^+ + \lambda_i^- \mathbf{P}_i^-) \cdot (\mathbf{a}_i \otimes \mathbf{N}_i) = 0, \quad i \in \mathcal{I}_G \quad (25)$$

where  $f_i$  is the configurational force which drives interfacial motion [14]. It bears emphasis that the leaf deformations  $\mathbf{F}_l$  may in general be arbitrarily away from the minima of  $W(\mathbf{F})$ , and thus the equilibrium equations (23) must be carefully enforced. In addition, the minimization (20)

has the effect of *optimizing* the volume fractions of all variants and the corresponding interface orientations. If all the preceding stationarity conditions are satisfied, then it is readily verified that the average or macroscopic deformation (17) is recovered as

$$\mathbf{P} = GW_{,\mathbf{F}}(\mathbf{F}) \quad (26)$$

which shows that  $GW(\mathbf{F})$  indeed supplies a potential for the average or macroscopic stress of the laminate.

The case in which the energy density  $W(\mathbf{F})$  possesses the multiwell structure (1) merits special mention. In this case, the minimization problem (20-22) may be written in the form:

$$GW(\mathbf{F}) = \inf_{\substack{\{\mathbf{a}_i, \lambda_i^\pm, \mathbf{N}_i, i \in \mathcal{I}_G\} \\ \{m_l \in \{1, \dots, M\}, l \in \mathcal{L}_G\}}} \sum_{l \in \mathcal{L}_G} \nu_l W_{m_l}(\mathbf{F}_l) \quad (27)$$

$$\lambda_i^\pm \in [0, 1], \quad i \in \mathcal{I}_G \quad (28)$$

$$|\mathbf{N}_i| = 1, \quad i \in \mathcal{I}_G \quad (29)$$

where  $\mathbf{m} = \{m_l \in \{1, \dots, M\}, l \in \mathcal{L}_G\}$  denotes the collection of wells which are active in each of the leaves. This problem may be conveniently decomposed into two steps: a first step involving energy minimization for a prescribed distribution of active wells, namely,

$$G_{\mathbf{m}}W(\mathbf{F}) = \inf_{\{\mathbf{a}_i, \lambda_i^\pm, \mathbf{N}_i, i \in \mathcal{I}_G\}} \sum_{l \in \mathcal{L}_G} \nu_l W_{m_l}(\mathbf{F}_l) \quad (30)$$

$$\lambda_i^\pm \in [0, 1], \quad i \in \mathcal{I}_G \quad (31)$$

$$|\mathbf{N}_i| = 1, \quad i \in \mathcal{I}_G \quad (32)$$

followed by the optimization of the active wells, i. e.,

$$GW(\mathbf{F}) = \inf_{\{m_l \in \{1, \dots, M\}, l \in \mathcal{L}_G\}} G_{\mathbf{m}}W(\mathbf{F}) \quad (33)$$

It should be carefully noted that the minimizers of problem (20-22) may be such that one or more of the volume fractions  $\lambda_i^\pm$  take the limiting values of 0 or 1. We shall say that a graph  $G$  is *stable* with respect to a macroscopic deformation  $\mathbf{F}$  if at least one minimizer of (20-22) is such that

$$\lambda_i^\pm \in (0, 1), \quad \forall i \in \mathcal{I}_G \quad (34)$$

and we shall say that the graph is *unstable* or *critical* otherwise. The presence of sub-trees of zero volume in an unstable graph is an indication that the graph is not ‘right’ for the macroscopic deformation  $\mathbf{F}$ , i. e., the graph is unable to support a nontrivial microstructure consistent with  $\mathbf{F}$ . Unstable graphs are mathematically contrived and physically inadmissible, and, as such, should be ruled out by some appropriate means. This exclusion may be accomplished, e. g., by the simple device of assigning the offending solutions an infinite energy, which effectively rules them out from consideration; or by defining solutions modulo *null* sub-trees, i. e., sub-trees of vanishing volume. In the present approach, we choose to integrate the exclusion of null sub-trees into the dynamics by which microstructures are evolved, as discussed next.

### 3.2 Microstructural evolution

The problem (20-22) may be regarded as a partial rank-one convexification of  $W(\mathbf{F})$  obtained by prescribing the graph  $G$  of the test laminates. The full rank-one convexification follows from the consideration of all possible graphs, i. e.,

$$RW(\mathbf{F}) = \inf_{G \in \mathcal{B}} GW(\mathbf{F}) \quad (35)$$

where, as before,  $\mathcal{B}$  is the set of all binary trees. In the particular case of energy densities of the form (1), we alternatively have

$$RW(\mathbf{F}) = \inf_{\substack{G \in \mathcal{B} \\ \{m_l \in \{1, \dots, M\}, l \in \mathcal{L}_G\}}} G_m W(\mathbf{F}) \quad (36)$$

It is clear that this problem exhibits combinatorial complexity as the rank of the test laminates increases, which makes a direct evaluation of (35) or (36) infeasible in general.

Problems of combinatorial complexity arise in other areas of mathematical physics, such as structural optimization and statistical mechanics. Common approaches to the solution of these problems are to restrict the search to the most ‘important’ states within phase space, or importance sampling; or to restrict access to phase space by the introduction of some form of dynamics. In this latter approach the states at which the system is evaluated form a sequence, or ‘chain’, and the next state to be considered is determined from the previous states in the chain. If, for instance, only the previous state is involved in the selection of the new state, a Markov chain is obtained. In problems of energy minimization, a common strategy is to randomly ‘flip’ the system and accept the flip with probability one if the energy is reduced, and with a small probability if the energy is increased.

In other cases, the system possesses some natural dynamics which may be exploited for computational purposes. A natural dynamics for problem (35) may be introduced as follows. Evidently, the relevant phase space for this problem is  $\mathcal{B}$ , the set of all binary trees, and the aim is to define a flow  $G(t)$  in this phase space describing the evolution of the microstructure along a *deformation processes*  $\mathbf{F}(t)$ . Here and subsequently, the real variable  $t \geq 0$  denotes time. A natural dynamics for  $G(t)$  is set by the following conditions:

1.  $G(t)$  must be stable with respect to  $\mathbf{F}(t)$ .
2.  $G(t)$  must be accessible from  $G(t^-)$  through a physically admissible transition.

The first condition excludes laminates containing null subtrees, i. e., subtrees of zero volume. The second criterion may be regarded as a set of rules for microstructural *refinement* and *unrefinement*.

In order to render these criteria in more concrete terms, we adopt an incremental viewpoint and seek to sample the microstructure at discrete times  $t_0 = 0, \dots, t_n, t_{n+1}, \dots$ . Suppose that the microstructure is known at time  $t_n$  and we are given a new macroscopic deformation  $\mathbf{F}_{n+1} = \mathbf{F}(t_{n+1})$ . In particular, let  $G_n$  be the graph of the microstructure at time  $t_n$ . We consider two classes of admissible transitions by which a new structure  $G_{n+1}$  may be reached from  $G_n$ :

1. The elimination of null subtrees from the graph of the laminate, or *pruning*.

## 2. The splitting of leaves, or *branching*.

Specifically, we refer to as branching the process by which a leaf is replaced by a simple laminate. The criterion that we adopt for accepting or rejecting a branching event is simple energy minimization. Thus, let  $l \in \mathcal{L}_{G_n}$  be a leaf in the microstructure at time  $t_n$ , and let  $\mathbf{F}_l^n$  be the corresponding deformation. The energetic ‘driving force’ for branching of the leaf  $l$  may be identified with

$$f_l^n = W(\mathbf{F}_l^n) - R_1 W(\mathbf{F}_l^n) \quad (37)$$

where  $R_1 W(\mathbf{F})$  is given by (6). We simply accept or reject the branching of the leaf  $l \in \mathcal{L}_{G_n}$  according as to whether  $f_l^n > 0$  or  $f_l^n \leq 0$ , respectively.

In the particular case in which  $W(\mathbf{F})$  is of the form (1), the evaluation of  $R_1 W(\mathbf{F})$  may be effected by considering all pairs of well energy densities, one for each variant. However, since the well energy densities  $W_m(\mathbf{F})$  are assumed to be quasiconvex and we rule out variants of zero volume, we may exclude from consideration the cases in which both variants of the laminate are in the same well. The evaluation of  $R_1 W(\mathbf{F})$  is thus reduced to the consideration of all distinct pairs of well energy densities.

The precise sequence of steps followed in calculations are as follows:

1. Initialization: Input  $\mathbf{F}_{n+1}$ , set  $G_{n+1} = G_n$ .
2. Equilibrium: Equilibrate laminate with  $G_{n+1}$  held fixed.
3. Evolution:
  - (a) Are there null subtrees?
    - i. YES : Prune all null subtrees, GOTO (2).
    - ii. NO : Continue.
  - (b) Compute all driving forces for branching  $\{f_l^{n+1}, l \in \mathcal{L}_{G_{n+1}}\}$ . Let  $f_{l_{\max}}^{n+1} = \max_{l \in \mathcal{L}_{G_{n+1}}} f_l^{n+1}$ .  
Is  $f_{l_{\max}}^{n+1} > 0$ ?
    - i. YES : Branch leaf  $l_{\max}$ , GOTO (2).
    - ii. NO : EXIT.

Several remarks are in order. The procedure just described may be regarded as a process of *continuation*, where the new microstructure is required to be close to the existing one in the sense just described. Evidently, since we restrict the class of microstructures which may arise at the end of each time step, there is no guarantee that this continuation procedure deliver the solution of (35) for all  $t \geq 0$ . However, metastability plays an important role in many systems of interest, and the failure to deliver the absolute rank-one convexification at all times is not of grave concern in these cases. Indeed, the continuation procedure described above may be regarded as a simple model of metastability.

In this regard, several improvements of the model immediately suggest themselves. Thus, the branching criterion employed in the foregoing simply rules out branching in the presence of an intervening energy barrier, no matter how small, separating the initial and final states. An

improvement over this model would be to allow, with some probability, for transitions requiring an energy barrier to be overcome, e. g., in the spirit of transition state theory and kinetic Monte Carlo methods. However, the implementation of this approach would require a careful and detailed identification of all the paths by which branching may take place, a development which appears not to have been undertaken to date.

## 4 Illustrative examples

As a first illustration of the sequential lamination algorithm presented in the foregoing, we apply it to a simple model of a Cu-Al-Ni shape-memory alloy, a material which has been extensively investigated in the literature (cf [7, 8, 22, 36], and references therein). Photomicrographs taken from the experiments of Chu and James [22] (also reported by [36]) reveal sharp laminated microstructures, often of rank two or higher. In order to exercise the algorithm, in the examples that follow we simply take the material through a prescribed macroscopic deformation path.

### 4.1 Material model

Cu-Al-Ni undergoes a cubic to orthorhombic martensitic transformation at around room temperature and has, therefore, six variants in the martensitic phase. The deformation undergone by the material in transforming from austenite to an unstressed variant of martensite may be described by a stretch tensor  $\mathbf{U}_m$ ,  $m = 1, \dots, 6$ . For Cu-Al-Ni, these are [22, 21]:

$$\mathbf{U}_1 = \begin{pmatrix} \zeta & 0 & 0 \\ 0 & \xi & \eta \\ 0 & \eta & \xi \end{pmatrix}, \quad \mathbf{U}_2 = \begin{pmatrix} \zeta & 0 & 0 \\ 0 & \xi & -\eta \\ 0 & -\eta & \xi \end{pmatrix}, \quad \mathbf{U}_3 = \begin{pmatrix} \xi & 0 & \eta \\ 0 & \zeta & 0 \\ \eta & 0 & \xi \end{pmatrix} \quad (38)$$

$$\mathbf{U}_4 = \begin{pmatrix} \xi & 0 & -\eta \\ 0 & \zeta & 0 \\ -\eta & 0 & \xi \end{pmatrix}, \quad \mathbf{U}_5 = \begin{pmatrix} \xi & \eta & 0 \\ \eta & \xi & 0 \\ 0 & 0 & \zeta \end{pmatrix}, \quad \mathbf{U}_6 = \begin{pmatrix} \xi & -\eta & 0 \\ -\eta & \xi & 0 \\ 0 & 0 & \zeta \end{pmatrix}. \quad (39)$$

where  $\xi = 1.0425$ ,  $\eta = 0.0194$  and  $\zeta = 0.9178$ , and all components are referred to the cubic axes of the austenitic phase. For purposes of illustration of the sequential lamination algorithm we adopt a simple energy density of the form (1), with well energy densities

$$W_0(\mathbf{F}) = \frac{1}{2}(\mathbf{F}^T \mathbf{F} - \mathbf{I}) \mathbb{C}_0 (\mathbf{F}^T \mathbf{F} - \mathbf{I}) \quad (40)$$

for the austenitic phase, and

$$W_m(\mathbf{F}) = \frac{1}{2}[(\mathbf{F}\mathbf{U}_m^{-1})^T(\mathbf{F}\mathbf{U}_m^{-1}) - \mathbf{I}] \mathbb{C}_m [(\mathbf{F}\mathbf{U}_m^{-1})^T(\mathbf{F}\mathbf{U}_m^{-1}) - \mathbf{I}], \quad m = 1, \dots, 6 \quad (41)$$

for the martensitic phases. In these expressions  $\mathbb{C}_m$ ,  $m = 0, \dots, M$ , are the elastic moduli at the bottom of the variants. These are (in MPa):

$$\mathbb{C}_0 = \begin{pmatrix} C_{11} & C_{12} & C_{12} & 0 & 0 & 0 \\ C_{12} & C_{11} & C_{12} & 0 & 0 & 0 \\ C_{12} & C_{12} & C_{11} & 0 & 0 & 0 \\ 0 & 0 & 0 & C_{33} & 0 & 0 \\ 0 & 0 & 0 & 0 & C_{33} & 0 \\ 0 & 0 & 0 & 0 & 0 & C_{33} \end{pmatrix} \quad (42)$$

where  $C_{11} = 141.76$ ,  $C_{12} = 126.24$  and  $C_{33} = 97$  and

$$\mathbb{C}_1 = \begin{pmatrix} C_{11} & C_{12} & C_{13} & 0 & 0 & 0 \\ C_{12} & C_{22} & C_{23} & 0 & 0 & 0 \\ C_{13} & C_{23} & C_{33} & 0 & 0 & 0 \\ 0 & 0 & 0 & C_{44} & 0 & 0 \\ 0 & 0 & 0 & 0 & C_{55} & 0 \\ 0 & 0 & 0 & 0 & 0 & C_{66} \end{pmatrix} \quad (43)$$

where  $C_{11} = 189$ ,  $C_{22} = 141$  and  $C_{33} = 205$ ,  $C_{12} = 124$ ,  $C_{13} = 45.5$ ,  $C_{23} = 115$ ,  $C_{44} = 54.9$ ,  $C_{55} = 19.7$ ,  $C_{66} = 62.6$  and with the moduli of the remaining martensitic variants following by symmetry. The energy density defined by (1) and (41) is material frame indifferent, results in stress-free states at the bottoms of all wells, i. e., at  $\mathbf{F} = \mathbf{I}$  and  $\mathbf{F} = \mathbf{R}\mathbf{U}_m$ ,  $\mathbf{R} \in SO(3)$ ,  $m = 1, \dots, 6$ , assigns equal energy density to all unstressed variants, and exhibits all the requisite material symmetries.

## 4.2 Optimization

In the examples presented here, and in the finite element calculations presented in the following section, problem (20-22) is solved using Spellucci's sequential quadratic programming (SQP) algorithm for constrained minimization. The SQP algorithm is an iterative procedure which requires an initial guess in order to start the iteration. In calculations we begin by setting the initial values of  $\{\mathbf{a}_i, \lambda_i^\pm, \mathbf{N}_i, i \in \mathcal{I}_{G_{n+1}}\}$  at time  $t_{n+1}$  equal to the converged values at time  $t_n$ . The main issue arises in evaluating possible branching events, as in this case new interfaces arise for which no previous geometrical information exists. The selection of initial guesses for  $\mathbf{a}_i$  and  $\lambda_i^\pm$ ,  $i \in \mathcal{I}_G$ , offers no difficulty, and we simply set  $\mathbf{a}_i = \mathbf{0}$  and  $\lambda_i^\pm = 0$  or 1. The choice of the initial value of the new interface normals  $\mathbf{N}_i$  requires more care since it strongly biases the resulting microstructure.

We have investigated two ways of initializing the normals  $\mathbf{N}_i$  arising during branching. A first approach is based on sampling the unit sphere uniformly. Thus, we simply select initial values of  $\mathbf{N}_i$  uniformly distributed over the unit sphere with some prespecified density and select the solution which results in the least energy. If two or more branched configurations possess the same energy, we select one at random. This exhaustive search approach is effective but costly owing to the large number of cases which need to be considered.

The second approach consists of priming the iteration using an initial guess derived from Ball and James [7, 8] constrained theory for shape-memory materials. In this theory, the elastic moduli are presumed large compared to the transformation stresses, so that the geometry of the laminate

wells	1	2	3	4	5	6
1		$e_3$	$e_1 - e_2$	$e_1 + e_2$	$e_1 - e_3$	$e_1 + e_3$
2	$e_2$		$e_1 + e_2$	$e_1 - e_2$	$e_1 + e_3$	$e_1 - e_3$
3	$e_1 - e_2$	$e_1 + e_2$		$e_3$	$e_2 - e_3$	$e_2 + e_3$
4	$e_1 + e_2$	$e_1 - e_2$	$e_3$		$e_2 + e_3$	$e_2 - e_3$
5	$e_1 - e_3$	$e_1 + e_3$	$e_2 - e_3$	$e_2 + e_3$		$e_2$
6	$e_1 + e_3$	$e_1 - e_3$	$e_2 + e_3$	$e_2 - e_3$	$e_1$	

Table 1: Vector  $e$  arising in the twinning relations for Cu-Al-Ni [17]. The vectors  $\{e_1, e_2, e_3\}$  correspond to the cube directions in the austenite phase.

can be obtained, to a first approximation, directly from the transformation strains. Conveniently, all resulting twinning relations between every distinct pair of martensitic wells can be tabulated beforehand. For Cu-Al-Ni this tabulation has been carried out by Bhattacharya, Li and Luskin [17]. As expected from general theory, the only non-trivial rank-one connections take place between distinct variants of martensite. Specifically, we seek  $Q \in SO(3)$ ,  $a, N \in \mathbb{R}^3$ ,  $|N| = 1$ , such that

$$QU_m = U_n + a \otimes N, \quad m, n = 1, \dots, 6, \quad m \neq n \quad (44)$$

There are two solutions to this equation. Let  $\tilde{e} = e/|e|$ , with the vector  $e$  as in Table 1. The first solution is

$$a = 2 \left( \frac{U_n^{-1} \tilde{e}}{|U_n^{-1} \tilde{e}|^2} - U_n \tilde{e} \right), \quad N = \tilde{e}, \quad n = 1, \dots, 6, \quad n \neq m \quad (45)$$

and the second solution is

$$a = CU_n \tilde{e}, \quad N = \frac{2}{C} \left( \tilde{e} - \frac{U_n^2 \tilde{e}}{|U_n^2 \tilde{e}|} \right), \quad C = 2 \left| \tilde{e} - \frac{U_n^2 \tilde{e}}{|U_n^2 \tilde{e}|} \right|, \quad n = 1, \dots, 6, \quad n \neq m \quad (46)$$

These results from the constrained theory may conveniently be used to start a branching calculation when the energy density is of the form (1). In this case, the branching calculation entails the consideration of every pair of well energy densities  $W_m(F)$  and  $W_n(F)$ ,  $m, n = 1, \dots, 6$ ,  $m \neq n$ , in the new leaves. The attendant iteration may then be started from the constrained solutions  $\{a, N\}$  described above, with the initial value of  $\lambda^\pm$  determined by means of a line search.

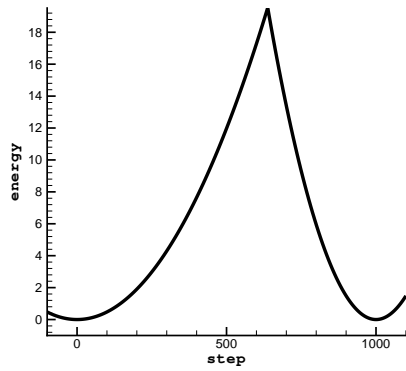
### 4.3 Martensite-martensite transition

Our first test case concerns the macroscopic deformation process

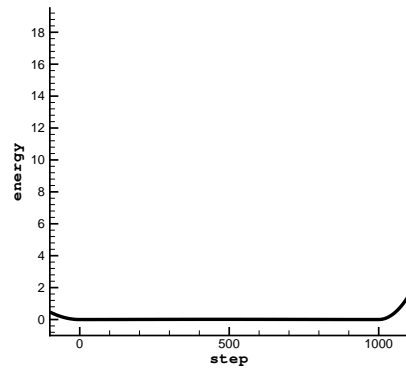
$$F(t) = (1 - t)U_1 + tU_2, \quad t \in [0, 1] \quad (47)$$

which takes the material from one variant of martensite to another. Fig. 3 shows the evolution of the energy, the component  $P_{13}$  of the first Piola-Kirchhoff stress, and the volume fraction  $\lambda$  of  $U_2$ , respectively, for the unrelaxed and relaxed cases. In this calculations, the branching constructions employ the constrained geometry as initial guess, as discussed in the foregoing.

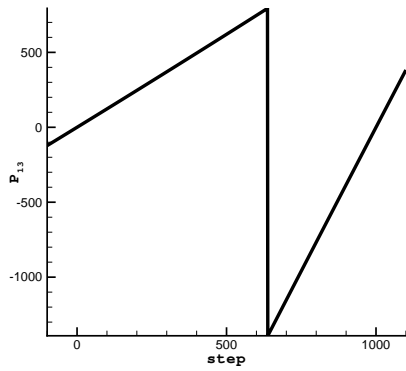
The unrelaxed response shown in Fig. 3 exhibits an abrupt transition from the initial to the final variant, as no mixed states are allowed to develop during the deformation process. By contrast, the



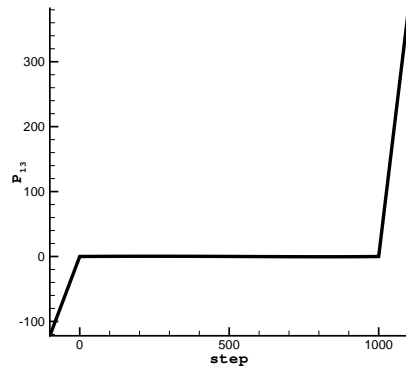
(a)



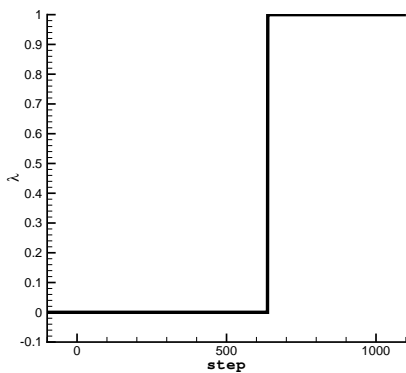
(b)



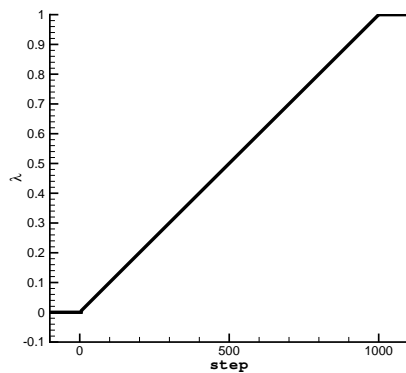
(c)



(d)



(e)



(f)

Figure 3: Martensite-to-martensite transition example. Comparison of unrelaxed (left) and relaxed (right) energies, stresses, and volume fractions.

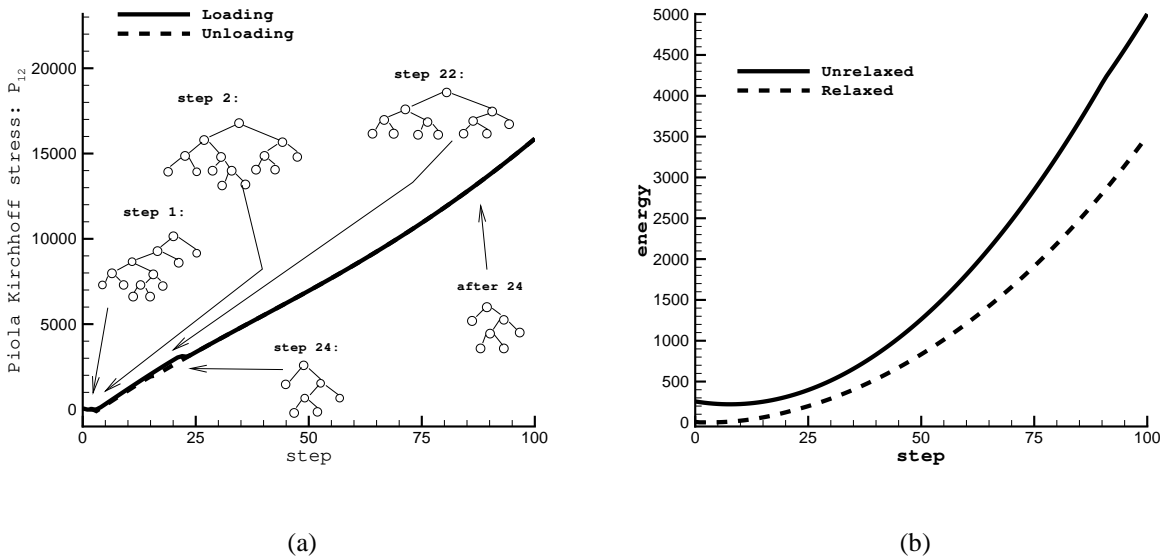


Figure 4: Simple shear example. a)  $P_{12}$  component of the first Piola-Kirchhoff stress tensor as a function of applied shear strain. The graph of the microstructures predicted by the relaxation algorithm are also shown inlaid. b) Unrelaxed and relaxed energies during loading.

relaxation algorithm results in the development of a rank-one laminate immediately following the onset of deformation. It should be carefully noted that the material is allowed to develop laminates of arbitrary rank, and that the persistency of a rank-one laminate is due to the fact that both leaves are stable against branching. The computed volume fraction  $\lambda$  increases linearly from 0 to 1. As a result of this evolving microstructure, the energy of the material is fully relaxed, and the material remains unstressed. In this example, the unloading response exactly traces in reverse the loading response, and hence no hysteresis is recorded.

#### 4.4 Simple shear

Our second test case concerns macroscopic simple shear on the plane (010) and in the direction (100). The material is taken to be initially undeformed, and the shear deformation is initially increased from zero up to a maximum value and then decreased to back zero. The calculations are carried out excluding the austenitic well from the definition (1) of the energy and considering the six martensitic wells only.

Fig. 4b shows a comparison of the computed unrelaxed and relaxed energies. By the exclusion of the austenitic well the material is forced to develop a rank-five laminate in its initial undeformed configuration. The graph of this laminate, and of all laminates which subsequently arise during deformation, is shown inlaid in Fig. 4a. As is evident from Fig. 4b, the relaxation algorithm ostensibly succeeds at fully relaxing the energy of the material. With increasing deformation, the computed microstructure undergoes transitions to rank-four and three laminates. A first rank-three

laminates of order thirteen is first predicted which subsequently simplifies to a rank-three laminate of order seven. As a result of this microstructural evolution, the relaxed energy remains well below the unrelaxed energy through the deformation, Fig. 4b. Upon unloading, the order-seven rank-three laminate is maintained down to zero deformation, suggesting that the initial microstructures computed during loading are metastable. Indeed, the unloading stress-strain curve lies below the loading one, resulting in a certain amount of hysteresis, which suggests that the order-seven rank-three laminate is indeed more efficient than the precursor microstructures.

## 5 Nonlocal extension

The simple branching criterion (37), which accounts for the energies of the variants only, neglects any energy barriers as may oppose the transformation and may lead to runaway refinement of the microstructure. In order to limit branching and, additionally, to estimate the size of the microstructure, we follow Ball and James [8] and take into consideration two additional sources of energy: the energy of the twin boundaries, and the mismatch energy contained within the boundary layers separating pairs of leaves. For instance, Boullay *et al.* [18], and James *et al.* [30] have investigated in detail the structure of branched needle microstructures that develop within the misfit boundary layers, e. g., at the edge of a martensite laminate. Such level of detail is well beyond the scope of this work. Our aim here is to derive a rough estimate of the misfit energy amenable to a straightforward calculation.

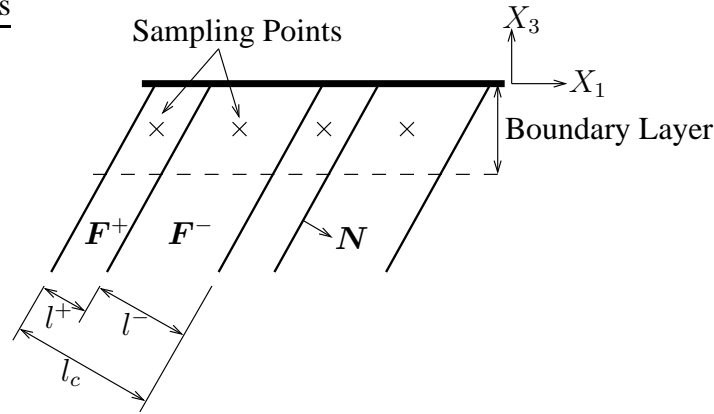


Figure 5: Schematic of interpolation boundary layer and scheme used to estimate misfit energy.

One such simple estimate may be derived as follows. Begin by enforcing ‘rigid-device’ boundary conditions

$$\mathbf{y}^{\text{BL}} = \mathbf{y}_0 + \bar{\mathbf{F}}(\mathbf{x} - \mathbf{x}_0), \quad x_3 = 0 \quad (48)$$

where  $\bar{\mathbf{F}}$  is the average deformation in the laminate,  $\mathbf{x}_0$  is a material point within the reference configuration of the laminate, and  $\mathbf{y}_0 = \mathbf{y}(\mathbf{x}_0)$  is its position on the deformed configuration. This insulates the laminate from the details of the adjacent deformation field in the regions  $x_3 > 0$  and  $x_3 < -l$ . A simple interpolating deformation mapping is then:

$$\mathbf{y}^{\text{BL}}(\mathbf{x}) = \mathbf{y}_0 - (\mathbf{y}(\mathbf{x}) - \mathbf{y}_0) \frac{x_3}{\Delta} + \bar{\mathbf{F}}(\mathbf{x} - \mathbf{x}_0) \left(1 + \frac{x_3}{\Delta}\right), \quad -\Delta \leq x_3 \leq 0 \quad (49)$$

where  $\mathbf{y}(\mathbf{x})$  is the deformation mapping of the laminate. The boundary layer at  $x_3 = -l$  can be given an identical treatment. The corresponding deformation mapping is

$$\mathbf{F}^{\text{BL}}(\mathbf{x}) = -\mathbf{F}(\mathbf{x})\frac{x_3}{\Delta} + \bar{\mathbf{F}}\left(1 + \frac{x_3}{\Delta}\right) + \frac{1}{\Delta}[\bar{\mathbf{F}}(\mathbf{x} - \mathbf{x}_0) - (\mathbf{y}(\mathbf{x}) - \mathbf{y}_0)] \otimes \mathbf{e}_3 \quad (50)$$

We proceed to estimate the elastic energy of the region defined by the intersection of each variant with the boundary layer by a simple one-point quadrature rule. Let  $\mathbf{x}^\pm$  be a pair of consecutive sampling points, Fig. 5, chosen such that  $x_3^\pm = -\Delta/2$ , and select  $\mathbf{x}_0 = \mathbf{x}^-$  for simplicity. Then, it follows immediately from (50) that

$$\mathbf{F}^{\text{BL}^-} \equiv \mathbf{F}^{\text{BL}}(\mathbf{x}^-) = \frac{1}{2}(\mathbf{F}^- + \bar{\mathbf{F}}) \quad (51)$$

Likewise,

$$\mathbf{F}^{\text{BL}^+} \equiv \mathbf{F}^{\text{BL}}(\mathbf{x}^+) = \frac{1}{2}(\mathbf{F}^+ + \bar{\mathbf{F}}) + [\bar{\mathbf{F}}(\mathbf{x}^+ - \mathbf{x}^-) - (\mathbf{y}^+ - \mathbf{y}^-)] \otimes \mathbf{e}_3 \quad (52)$$

But, since  $\mathbf{y}(\mathbf{x})$  is piecewise linear, it follows that

$$\mathbf{y}^+ - \mathbf{y}^- = \mathbf{F}^-(\lambda^-(\mathbf{x}^+ - \mathbf{x}^-)) + \mathbf{F}^+(\lambda^+(\mathbf{x}^+ - \mathbf{x}^-)) = \bar{\mathbf{F}}(\mathbf{x}^+ - \mathbf{x}^-) \quad (53)$$

and

$$\mathbf{F}^{\text{BL}^+} = \frac{1}{2}(\mathbf{F}^+ + \bar{\mathbf{F}}) \quad (54)$$

Collecting the above results we finally have

$$\mathbf{F}^{\text{BL}^\pm} = \frac{1}{2}(\mathbf{F}^\pm + \bar{\mathbf{F}}) \quad (55)$$

Within this approximation, the misfit boundary-layer energy density finally evaluates to

$$W^{\text{BL}} = \lambda^- [W(\mathbf{F}^{\text{BL}^-}) - W(\mathbf{F}^-)] + \lambda^+ [W(\mathbf{F}^{\text{BL}^+}) - W(\mathbf{F}^+)] \quad (56)$$

which furnishes a remarkably simple (though rough) estimate. We note that

$$\mathbf{F}^{\text{BL}^+} - \mathbf{F}^{\text{BL}^-} = \frac{1}{2}(\mathbf{F}^+ - \mathbf{F}^-) = \frac{1}{2}\mathbf{a} \otimes \mathbf{N} \quad (57)$$

and

$$\lambda^- \mathbf{F}^{\text{BL}^-} + \lambda^+ \mathbf{F}^{\text{BL}^+} = \bar{\mathbf{F}} \quad (58)$$

Thus, the deformations  $\mathbf{F}^{\text{BL}^\pm}$  are rank-one compatible and match the average deformation of the laminate. Since the deformations  $\mathbf{F}^\pm$  minimize the energy of the laminate among all rank-one laminates with average deformation  $\bar{\mathbf{F}}$ , it follows that  $W^{\text{BL}} \geq 0$ , i. e.,  $W^{\text{BL}}$  does indeed represent an *excess energy*.

For simplicity, we assume that the twin-boundary energy  $\Gamma$  per unit area is a constant independent of the deformation of the variants. Combining the preceding estimates, it follows that total

excess or *nonlocal* energy due to the twin boundaries and the misfit boundary layers contained within a region of the laminate of dimensions  $L \times L \times l$  is:

$$E^{\text{NL}} = L^2 l \left\{ \frac{\Gamma}{l^c} + \frac{2\Delta}{l} W^{\text{BL}} \right\} \quad (59)$$

Taking  $\Delta = l^c/2$ , for definiteness, this expression reduces to

$$E^{\text{NL}} = L^2 l \left\{ \frac{\Gamma}{l^c} + \frac{l^c}{l} W^{\text{BL}} \right\} \quad (60)$$

This excess energy may now be minimized with respect to  $l^c$ , with the result:

$$l^c = \sqrt{\frac{\Gamma l}{W^{\text{BL}}}} \quad (61)$$

which affords an estimate of  $l^c$ . The corresponding minimum excess energy per unit volume is

$$W^{\text{NL}} \equiv \frac{E^{\text{NL}}}{L^2 l} = 2\sqrt{\frac{\Gamma W^{\text{BL}}}{l}} \quad (62)$$

We note that this excess energy grows as  $l^{-1/2}$ , which tends to suppress microstructural refinement. In calculations, we interpret the excess energy density  $W^{\text{NL}}$  as an energy barrier for branching. Consideration of this energy barrier has the effect of reducing the local branching driving force (37) to

$$f_l^n = W(\mathbf{F}_l^n) - R_1 W(\mathbf{F}_l^n) - W^{\text{NL}}(\mathbf{F}_l^n) \quad (63)$$

which effectively introduces a lower cut-off for the size of the microstructure and eliminates the possibility of runaway microstructural refinement.

## 6 Application to the finite-element simulation of indentation in Cu-Al-Ni

The sequential lamination algorithm developed in the foregoing may conveniently be taken as a basis for multiscale simulation in situations in which there is a strict separation of scales: a macroscopic scale characterized by slowly-varying smooth fields; and a much smaller scale commensurate with the size of the evolving microstructure. As remarked by several authors [20, 36, 19, 24], these problems may be solved effectively by pushing the microstructure to the *sub-grid* scale, while solving the well-posed relaxed problem on the computational grid.

In this section we present selected examples of application of this multiscale approach in which the macroscopic problem is solved by the finite-element method, while the effective behavior is computed, simultaneously with the macroscopic solution, at the Gauss-point level using the sequential lamination algorithm developed in the foregoing. The particular problem considered concerns the quasistatic normal indentation of a Cu-Al-Ni shape-memory alloy by a spherical indenter. The domain of analysis and the computational mesh are shown in Fig. 6. The analysis is reduced to one quarter of the entire domain for simplicity. In particular, solutions exhibiting broken symmetry

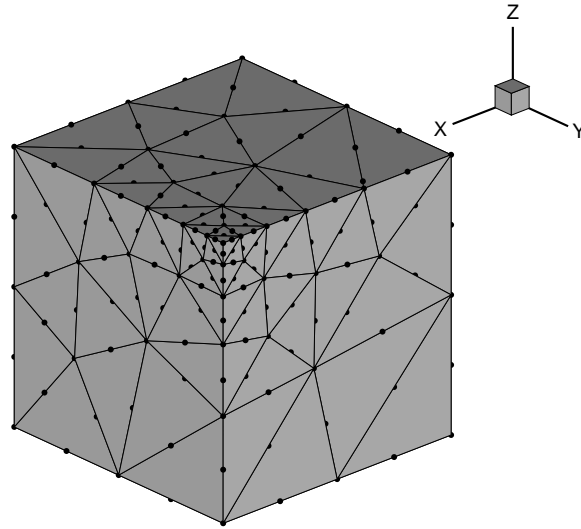


Figure 6: *Computational domain and finite element mesh.*

are ruled out by the analysis. The size of the computational domain is  $20\text{mm} \times 20\text{mm} \times 20\text{mm}$ . The radius of the indenter is  $15\text{mm}$ . The specimen is fully supported over its entire base, and the remainder of its boundary is free of tractions. The computational mesh contains 254 nodes and 105 ten-node quadratic tetrahedral elements. Contact between the indenter and the specimen is assumed to be frictionless and is enforced by a penalty method [43]. To ensure that the jacobian  $J$  of the deformation remains positive in all variants at all times, the energy of each well is augmented by a term of the form [38]

$$W^{\text{vol}}(J) = \begin{cases} C(J^2 + J^{-2} - 2)^2, & J < 1 \\ 0, & \text{otherwise} \end{cases} \quad (64)$$

where  $C$  is a constant chosen sufficiently small to minimize the effect on the total energy. By design,  $W^{\text{vol}}(J)$  and its first and second derivatives vanish at  $J = 1$ . In addition, the twin-boundary and misfit energies are accounted for as part of the branching criterion as a means of introducing a lower cutoff for the laminate size and preventing runaway microstructural refinement. In all calculations, the twin-boundary energy per unit area  $\Gamma$  is set to  $1 \text{ J/m}^2$ . The maximum size of the laminate at a particular Gauss point is set to the element size, in keeping with the assumption that the laminate accounts for sub-grid structure in the solution only, and that coarser structures are adequately resolved by the mesh.

The finite-element solution is obtained by dynamic relaxation followed by a preconditioned conjugate-gradient iteration [45]. The high level of concurrency in the constitutive calculations was exploited via an MPI-based parallel implementation [42] on the ASCI Blue multiprocessing computer. Performance studies showed excellent load balancing and scalability.

Fig. 7 shows the *unrelaxed* deformed configurations, and the corresponding distribution of active energy wells at the Gauss points of the mesh, at depths of indentation of  $0.150$  and  $0.375 \text{ mm}$ .

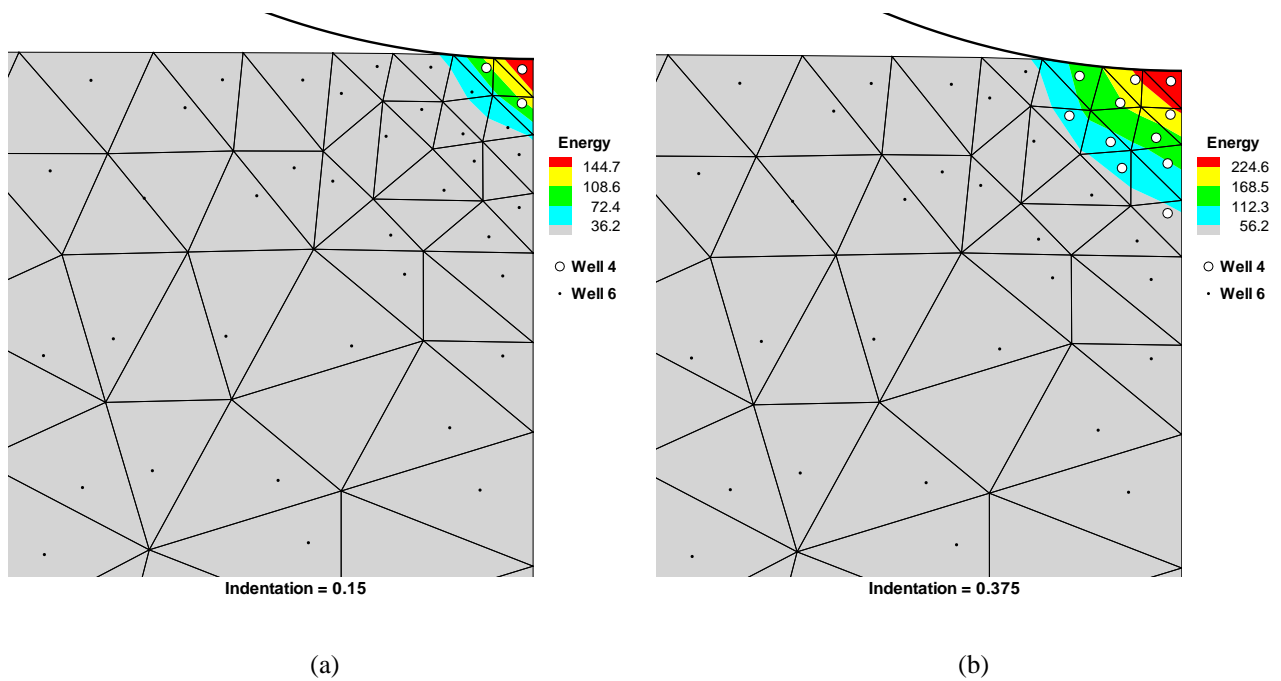


Figure 7: Cross-sections and energy-density contours for two unrelaxed solutions at depths of indentation: a) 0.150 mm, and b) 0.375 mm. The symbols designate the energy well which is activated at each Gauss point of the mesh.

As is evident from this figure, two energy wells become active during indentation. The transformed zone under the indenter grows with depth of indentation, but the fineness of the variant arrangement is severely limited by the mesh size. Correspondingly, the total energies and indentation forces recorded during indentation are comparatively high, Fig. 9. In this figure the energy has been normalized by  $E_0 = V_0 C_{11}^{Austenite}$ , where  $V_0$  is the volume of the undeformed specimen, while the force has been normalized by  $F_0 = E_0/R_{Indenter}$ .

The *relaxed* solution obtained using the sequential lamination algorithm differs markedly from the unrelaxed solution just described, Fig. 8. Thus, the relaxed deformation field is accompanied by the development of well-defined microstructures at the subgrid level. Some of the laminates generated by the sequential lamination algorithm are quite complex, reaching rank two. Of note is the appearance of a de-twinned zone directly under the indenter. The effect of relaxation on the total energy and indentation force is quite marked, Fig. 9, with the relaxed values lying well below the unrelaxed ones. Unloading exhibits the path-dependent nature of the algorithm, with the microstructure established at maximum load remaining in place during much of the unloading process, which in turn results in a soft response. The fineness of the microstructure is somewhat overpredicted by the calculations, with some of the variants attaining sub-micron thicknesses. In view of (61), this excessive refinement may owe to a low value of the twin-boundary energy  $\Gamma$ , or to an overestimation of the misfit energy  $W^{BL}$ , or both.

## 7 Summary and Concluding Remarks

We have presented a practical algorithm for partially relaxing multiwell energy densities. The algorithm is based on sequential lamination, but it is constrained in such a way that successive microstructures occurring along a deformation path are close to each other in a certain sense: the new microstructure should be reachable from the preceding one by a combination of branching and pruning operations. All microstructures generated by the algorithm are in static and configurational equilibrium. In particular, we optimize all the interface orientations and variant volume fractions, with the result that all configurational forces and torques are in equilibrium. We additionally allow the variants to be arbitrarily stressed and enforce traction equilibrium across all interfaces. Owing to the continuity constrained imposed upon the microstructural evolution, the predicted material behavior may be path-dependent and exhibit hysteresis.

In cases in which there is a strict separation of micro and macrostructural lengthscales, the proposed relaxation algorithm may effectively be integrated into macroscopic finite-element calculations at the subgrid level. We have demonstrated this aspect of the algorithm by means of a numerical example concerned with the indentation of an Cu-Al-Ni shape memory alloy [22] by a spherical indenter. The calculations illustrate the ability of the algorithm to generate complex microstructures, resulting in force-depth of indentation curves considerably softer than otherwise obtained by direct energy minimization.

Several improvements of the present approach immediately suggest themselves. The relaxation algorithm, in its present form, does not account for energy barriers for branching. Thus, a significant improvement over this model would be to permit, with probability less than one, transitions

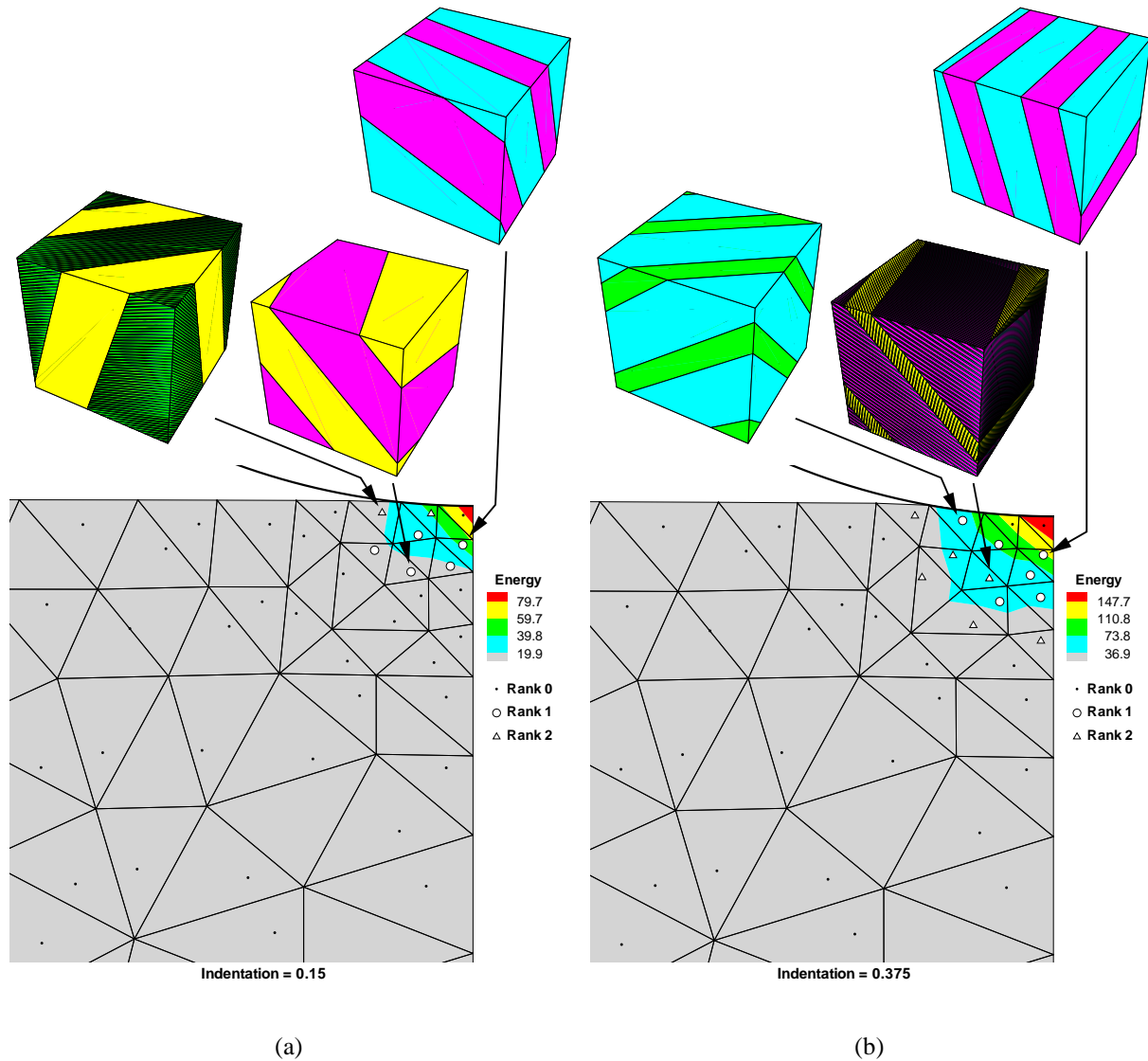


Figure 8: Cross-section and energy-density contours for relaxed solution at an indentation depth of: a) 0.150 mm, and b) 0.375 mm. The symbols indicate the rank of the microstructure at the Gauss points. The insets depict the geometry of the microstructure at the indicated sampling points, with each color representing an individual well, and are of identical size oriented such that the left face corresponds to the cross-section plane.

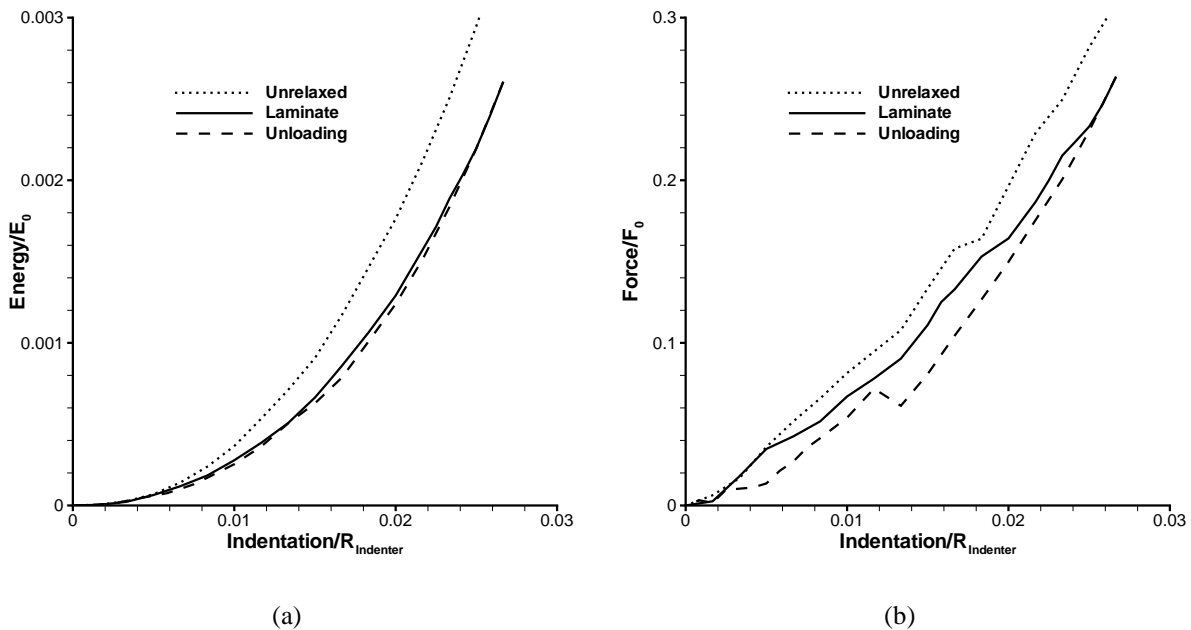


Figure 9: Normalized total energy vs. normalized depth of indentation; b) Normalized indentation force vs. normalized depth of indentation.

requiring an energy barrier to be overcome, e. g., in the spirit of transition state theory and kinetic Monte Carlo methods. This extension would require a careful and detailed identification of all the paths by which branching may take place, and the attendant energy barriers. Another significant improvement would be to relax the configurational force equilibrium constraint and replace it by a kinetic relation governing interfacial motion [1, 2, 14]. Kinetic relations of this form can effectively be integrated into the variational principle with the aid of time discretization [39, 41].

## Acknowledgments

We are grateful for support provided by the US Department of Energy through Caltech's ASCI/ASAP Center for the Simulation of the Dynamic Behavior of Solids; and for support provided by the AFOSR through Brown's MURI for the Design of Materials by Computation. MF is also grateful for support provided by the DOE and Krell Institute through a Computational Science Graduate Fellowship.

## References

- [1] R. Abeyaratne, C. Chu, and R. D. James. Kinetics of materials with wiggly energies: theory and application to the evolution of twinning microstructures in a Cu-Al-Ni shape memory alloy. *Philosophical Magazine A*, 73(2):457–497, 1996.

- [2] R. Abeyaratne and J.K. Knowles. On the kinetics of an austenite->martensite phase transformation induced by impact in a Cu-Al-Ni shape-memory alloy. *Acta Materialia*, 45(4):1671–1683, 1997.
- [3] E. Aranda and P. Pedregal. Numerical approximation of non-homogeneous, non-convex vector variational problems. *Numerische Mathematik*, 89(3):425–444, 2001.
- [4] E. Aranda and P. Pedregal. On the computation of the rank-one convex hull of a function. *SIAM Journal on Scientific Computing*, 22(5):1772–1790, 2001.
- [5] S. Aubry, K. Bhattachatya, and M. Ortiz. Effective behavior of single crystals. to be submitted.
- [6] S. Aubry and M. Ortiz. Latent hardening and dislocation structures in crystals. *to appear*, 2001.
- [7] J. Ball and R. D. James. Proposed experimental tests of a theory of fine microstructure and the two-well problem. *Phil. Trans. R. Soc. Lond.*, 338:389–450, 1992.
- [8] J. Ball and R. D. James. Fine phase mixtures as minimizers of energy. *Z. Angew. Math. Mech.*, 76:389–392, 1996.
- [9] J. M. Ball, C. Chu, and R. D. James. Hysteresis during stress-induced variant rearrangement. *Journal de physique IV*, 5:245–251, 1995. Colloque C8, supplément au journal de physique III.
- [10] S. Bartels, C. Carstensen, P. Plecháč, and A. Prohl. Finite element computation of macroscopic quantities in nonconvex minimization in micromagnetics and materials science. to appear.
- [11] K. J. Bathe. *Finite Element Procedures*. Prentice Hall, 1995.
- [12] K. Bhattacharya. Wedge-like microstructure in martensites. *Acta metall*, 39:2431–2444, 1991.
- [13] K. Bhattacharya. Self-accommodation in martensites. *Arch. Rat. Mech. Anal.*, 120:201–244, 1992.
- [14] K. Bhattacharya. Comparison of the geometrically nonlinear and linear theories of martensitic transformations. *Continuum Mechanics and Thermodynamics*, 5:205–242, 1993.
- [15] K. Bhattacharya, R. D. James, and P. J. Swart. Relaxation in shape-memory alloys-part i. mechanical model. *Acta mater.*, 45(11):4547–4560, 1997.
- [16] K. Bhattacharya, R. D. James, and P. J. Swart. Relaxation in shape-memory alloys-part ii. thermo-mechanical model and proposed experiments. *Acta mater.*, 45(11):4561–4568, 1997.
- [17] K. Bhattacharya, B. Li, and M. Luskin. Simply laminated microstructure. *Arch. Rational Mech. Anal.*, 149:123–154, 1999.

- [18] P. Boullay, D. Schryvers, and R. V. Kohn. Bending martensite needles in Ni<sub>65</sub>Al<sub>35</sub> investigated by two-dimensional elasticity and high-resolution transmission electron microscopy - art. no. 144105. *Physical Review B*, 64(14):4105, 2001.
- [19] C. Carstensen and P. Plecháč. Numerical solution of the scalar double-well problem allowing microstructure. *Math. Comput.*, 66(219):997–1026, 1997.
- [20] M. Chipot and D. Kinderlehrer. Equilibrium configurations of crystals. *Arch. Rat. Mech. Anal.*, 103:237–277, 1988.
- [21] C. Chu. *Hysteresis and microstructures: A study of biaxial loading on compound twins of copper-aluminum-nickel single crystals*. PhD thesis, University of Minnesota, 1993.
- [22] C. Chu and R. D. James. Analysis of microstructures in Cu-14.0% Al-3.9% Ni by energy minimization. *Journal de physique IV*, 5:143–149, 1995.
- [23] R. Dacorogna. *Direct methods in the calculus of variations*. Springer-Verlag Berlin, 1989.
- [24] A. DeSimone. Energy minimizers for large ferromagnetic bodies. *Arch. rat. Mech. Anal.*, 125:99–143, 1993.
- [25] G. Dolzmann. Numerical computation of rank-one convex envelopes. *SIAM J. Numer. Anal.*, 36(5):1621–1635, 1999.
- [26] J. Eriksen. Some phase transitions in crystals. *Arch. Rat. Mech. Anal.*, 73:99–124, 1980.
- [27] S. Govindjee and C. Miehe. A multi-variant martensitic phase transformation model: formulation and numerical implementation. *Computer Methods in Applied Mechanics and Engineering*, 191(3-5):215–238, 2001.
- [28] T. J. R. Hughes. *The Finite Element Method: Linear Static and Dynamic Finite Element Analysis*. Dover Publications, 2000.
- [29] R. D. James and D. Kinderlehrer. Theory of diffusionless phase transitions. In Springer, editor, *PDEs and continuum models of phase transitions*, number 344 in Lecture Notes in Physics. M. Rascle, D. Serre and M. Slemrod, eds., 1989.
- [30] R. D. James, R. W. Kohn, and T. W. Shield. Modeling of branched needle microstructures at the edge of a martensite laminate. *Journal de Physique IV*, 5(C8):253–259, 1995.
- [31] R.V. Kohn. Relaxation of a double-well energy. *Cont. Mech and Thermodyn.*, 3:193–236, 1991.
- [32] R.V. Kohn and G. Strang. Explicit relaxation of a variational problem in optimal-design. *Bulletin of the American Mathematical Society*, 9(2):211–214, 1983.
- [33] R.V. Kohn and G. Strang. Optimal design and relaxation of variational problems i-ii-iii. *Comm. Pure Appl. Math.*, 39:113–137, 139–182, 353–377, 1986.

- [34] M. Kruzik. Numerical approach to double well problems. *SIAM Journal on Numerical Analysis*, 35(5):1833–1849, 1998.
- [35] B. Li and M. Luskin. Approximation of a martensitic laminate with varying volume fractions. *Mathematical Modelling and Numerical Analysis M2AN*, 33(1):67–87, 1999.
- [36] M. Luskin. On the computation of crystalline microstructure. *Acta Numer.*, 5:191–257, 1996.
- [37] S. Müller. Variational models for microstructure and phase transitions. Technical report, Max-Planck Intitute, 1998.
- [38] P. Neff. Suitable energy functionals to limit jacobian. Personal communication, 2001.
- [39] M. Ortiz and E. A. Repetto. Nonconvex energy minimization and dislocation structures in ductile single crystals. *J. Mech. Phys. Solids*, 47(2):397–462, 1999.
- [40] M. Ortiz, E. A. Repetto, and L. Stainier. A theory of subgrain dislocation structures. preprint submitted to Elsevier preprint.
- [41] M. Ortiz and L. Stainier. The variational formulation of viscoplastic constitutive updates. *Comput. Methods Appl. Mech. Engrg.*, 171:419–444, 1999.
- [42] P. Pacheco. *Parallel Programming with MPI*. Morgan Kaufmann, 1996.
- [43] A. Pandolfi. Inpenetrability constraints. Unpublished, 2001.
- [44] P. Pedregal. Laminates and microstructure. *Europ. J. Appl. Math.*, 4:121–149, 1993.
- [45] J. R. Shewchuk. An introduction to the conjugate gradient method without the agonizing pain. <http://www.cs.cmu.edu/~quake-papers/painless-conjugate-gradient.ps>, 1994.
- [46] P. Spellucci. A new technique for inconsistent qp problems in the sqp method. *Math. Method. Oper. Res.*, 47(3):355–400, 1998.
- [47] A. E. Giannakopoulos T. A. Venkatesh, K. J. Van Vliet and S. Suresh. Determination of elasto-plastic properties by instrumented sharp indentation: guidelines for property extraction. *Scripta Mater.*, 42(9):833–839, 2000.
- [48] E. B. Tadmor, G. S. Smith, N. Bernstein, and E. Kaxiras. Mixed finite element and atomistic formulation for complex crystals. *Physical review B*, 59(1):235–245, 1999.
- [49] E. B. Tadmor, U. V. Waghmare, G. S. Smith, and E. Kaxiras. Polarization switching in  $\text{PbTiO}_3$ : an ab initio finite element simulation. to be submitted to *Acta Materialia*.
- [50] A. E. Giannakopoulos U. Ramamurty, S. Sridhar and S. Suresh. An experimental study of spherical indentation of piezoelectric materials. *Acta Mater.*, 47(8):2417–2430, 1999.
- [51] O. C. Zienkiewicz and R. L. Taylor. *Finite Element Method: Volume 1, The Basis*. Butterworth-Heinemann, 2000.
- [52] O. C. Zienkiewicz and R. L. Taylor. *Finite Element Method: Volume 2, Solid Mechanics*. Butterworth-Heinemann, 2000.